DPP-4 Inhibitors Improve Diabetic Wound Healing via Direct and Indirect Promotion of Epithelial-Mesenchymal Transition and Reduction of Scarring

Min Long,[1] Leiqin Cai,[1] Wenjie Li,[1] Linlin Zhang,[1] Shaodong Guo,[2] Rui Zhang,[1] Yi Zheng,[1] Xiufei Liu,[1] Min Wang,[1] Xianli Zhou,[1] Hui Wang,[1] Xing Li,[1] Ling Li,[3] Zhiming Zhu,[4] Gangyi Yang,[5] and Hongting Zheng[1]

Diabetes 2018;67:518–531 | https://doi.org/10.2337/db17-0934

COMPLICATIONS

Patients with diabetes often experience multiple disease complications. Hypoglycemic agents can have both positive and negative effects on diabetic complications, which should be carefully assessed when personalized treatment strategies are developed. In this study we report that dipeptidyl peptidase 4 inhibitors (DPP-4is), a group of widely used antihyperglycemic agents, can improve diabetic wound healing, independent of their beneficial effects on glycemic control. In particular, DPP-4is promoted the migration and epithelial-mesenchymal transition of keratinocytes, directly and indirectly, by inducing stromal cell-derived factor 1α production of fibroblasts in vitro and in diabetic mice. In addition, DPP-4is attenuated collagen synthesis and deposition, which may diminish scar formation. Furthermore, the results of a randomized clinical trial (NCT02742233) involving 67 patients with type 2 diabetes supported the role of DPP-4i treatment in diabetic wound healing. Our findings support the application of DPP-4i as a preferred option for treating ulcers in patients with diabetes.

Various complications occur frequently in diabetes, but how to choose optimal personalized hypoglycemic agents is not completely clear because these agents may have additional effects on these complications. On one hand, for instance, liraglutide has been shown to bring cardiovascular benefits (1), dapagliflozin has antihypertensive effects (2), and metformin can reduce maternal weight gain without lowering infant birth weight (3). On the other hand, some hypoglycemic agents also cause negative side effects, such as the increased risk of heart failure hospitalization that is associated with saxagliptin (Sax) (4,5) and the elevated renal failure incidence with dapagliflozin (6). These results have begun to influence the selection of hypoglycemic agents. Therefore, an improved understanding of the additional effects of hypoglycemic agents is required to optimize individualized clinical treatment.

Dipeptidyl peptidase 4 inhibitors (DPP-4is) are classic antihyperglycemic agents used worldwide and are recommended as the first-line treatment for patients with type 2 diabetes (T2D) by the American Association of Clinical Endocrinologists (7) owing to their efficacy in glycemic control and the minimum risk of hypoglycemia. Traditionally, DPP-4i is believed to reduce levels of hemoglobin A_{1c} (HbA_{1c}) by prolonging the half-life of endogenous glucagon-like peptide 1 (GLP-1) and glucose-dependent insulinotropic polypeptide (8), which are normally cleaved into inactive forms during circulation by plasma DPP-4 upon recognition of the X-proline dipeptides present on their N-terminals. However, in addition to the hypoglycemic effects, several studies have indicated that DPP-4i may have additional effects on the kidney (9,10) and cardiovascular system (11). Recently, DPP-4i was demonstrated to activate the nuclear factor-E2–related factor 2 (NRF2)

[1]Department of Endocrinology, Translational Research Key Laboratory for Diabetes, Xinqiao Hospital, Third Military Medical University, Chongqing, China
[2]Department of Nutrition and Food Science College of Agriculture and Life Sciences, Texas A&M University, College Station, TX
[3]Department of Clinical Biochemistry, College of Laboratory Medicine, Chongqing Medical University, Chongqing, China
[4]Department of Hypertension and Endocrinology, Daping Hospital, Third Military Medical University, Chongqing, China
[5]Department of Endocrinology, The Second Affiliated Hospital, Chongqing Medical University, Chongqing, China

Corresponding author: Hongting Zheng, fnf7703@hotmail.com.

Received 8 August 2017 and accepted 7 December 2017.

Clinical trial reg. no. NCT02742233, clinicaltrials.gov.

This article contains Supplementary Data online at http://diabetes.diabetesjournals.org/lookup/suppl/doi:10.2337/db17-0934/-/DC1.

M.L. and L.C. contributed equally to this work.

pathway (12,13), a vital cellular defense pathway in response to oxidative stress (14,15). Our and other groups have shown that NRF2 is relevant to diabetic wound healing (16,17), which suggested that DPP-4is may also influence diabetic wound repair. In fact, as the target of DPP-4is, DPP-4 (also called CD26) has been reported to be involved in a multitude of tissue repair processes. This enzyme is widely expressed by many types of cells, such as normal epithelial cells, tumor cells, and immune cells, and displays diverse biological functions (18–20). DPP-4 can take part in regulation of tissue regeneration by affecting angiogenesis, cell survival, and proliferation through its substrates, such as GLP-1 and interferon-γ–inducible protein 10 (IP-10) (21,22). Its immunomodulatory function has also been identified to contribute to tissue repair by regulating lymphocyte T-cell activation and monocyte/macrophage recruitment (22,23).

Given the multitude of potential roles that DPP-4 can play, we hypothesize that DPP-4i may also have effects on diabetic wound healing. We considered the possibilities of DPP-4i indirectly influencing diabetic wound healing as an environmental modifier that decreases oxidative stress or as a more direct modifier of cell-intrinsic behavior. In this study, we investigated the effects of DPP-4is in vitro and in vivo using an animal model and then validated the results in a clinical trial. Potential mechanisms involving multiple cells and different stages of the wound healing process were explored. Our results revealed an obvious positive effect of DPP-4is on diabetic wound healing, independent of glycemic control. Importantly, we found that the effect of DPP-4i is not mainly through the NRF2 pathway; instead, it promotes the epithelial-mesenchymal transition (EMT) of keratinocytes directly, indirectly drives EMT by enhancing the stromal cell-derived factor 1α (SDF-1α) expression of fibroblasts, and reduces scarring.

RESEARCH DESIGN AND METHODS

Cell Culture and Reagents

Human immortalized keratinocytes (HaCaT cells) were obtained from the Institute of Basic Medical Sciences, Peking Union Medical College, and cultured in RPMI-1640 medium (Gibco) with 10% FBS. Human foreskin fibroblasts (HFFs) were purchased from the cell bank of Chinese Academy of Sciences and grown in DMEM (Gibco) with 10% FBS, 1 mmol/L sodium pyruvate (Gibco), GlutaMAX-1 (Gibco), and 1% minimum essential medium nonessential amino solution (HyClone). Both cell lines were authenticated with short tandem repeat profiling (Federal Bureau of Investigation, Combined DNA Index System) and were free of mycoplasma contamination based on quantitative (q)RT-PCR and cultures. Cells were maintained at 37°C in a humidified atmosphere under 5% CO_2. The compounds Sax and sitagliptin (Sit) were obtained from Beijing Huikang Boyun and BioVision. The commercial human drugs Sax (Bristol-Myers Squibb), Sit (Merck Sharp & Dohme), alogliptin (Alo) (Meiji Yakuhin Co.), linagliptin (Lin) (Boehringer Ingelheim International GmbH), and vildagliptin (Vil) (Novartis Europharm) were also used. Streptozotocin (Sigma-Aldrich), SDF-1α (PeproTech), and transforming growth factor (TGF)-β1 (Sino Biological) were purchased. The primary antibody used for immunohistochemistry (IHC) analysis was anti–SDF-1α (R&D). Primary antibodies for immunofluorescence and Western blot included anti–E-cadherin (Cell Signaling Technology), anti-vimentin (Santa Cruz Biotechnology and R&D), anti-SNAIL1, anti–vascular endothelial growth factor (VEGF), anti–TGF-β1, anti–cyclooxygenase 2 (COX2), and anti–β-actin (Santa Cruz Biotechnology), as well as anti–high mobility group box 1 (HMGB1), and anti–SDF-1α (Abcam). All horseradish peroxidase (HRP)-conjugated secondary antibodies (ZB-2301, ZB-2305) were obtained from ZSGB-Bio. The anti–mouse-IgG conjugated with Alexa Fluor 488, anti–rabbit-IgG conjugated with Alexa Fluor 647, anti–rabbit-IgG conjugated with Cy3, and DAPI were purchased from Beyotime Biotechnology. The anti–rat-IgG conjugated with Alexa Fluor 488 was obtained from Biosynthesis Biotechnology.

qRT-PCR and Western Blot

The skin tissues of mice were homogenized in TRIzol reagent (TIANGEN) using a tissue homogenate apparatus (Bertin Precellys 24), and the total RNA of the mouse wound skin tissues and cells was extracted according to the manufacturer's instructions. RNA quality was assessed with a NanoDrop2000 spectrophotometer (Thermo Scientific) by examining the 260-to-280 ratio. Samples with a ratio of 1.8–2.0 were processed to reverse-transcribe into cDNA by using a Prime Script RT reagent Kit (TaKaRa). The transcript levels of the target genes were analyzed by qRT-PCR performed with the SYBR Premix Ex Taq II (TaKaRa) in an Applied Biosystems 7300 system (Life Technologies). The primers included in our study are listed in Supplementary Table 2, and GAPDH mRNA expression served as the normalization reference.

Western blot was performed as previously described (12). Briefly, cells were harvested in sample buffer (2% SDS, 50 mmol/L Tris-HCl [pH 6.8], 100 mmol/L dithiothreitol, 10% glycerol, and 0.1% bromophenol blue), boiled at 98°C for 5 min, and sonicated with an ultrasonic cell crusher (SJIALAB) for 2 min at 10% intensity, and protein concentrations were determined by an RC DC Protein Assay kit (Bio-Rad). Cell lysates underwent SDS-PAGE and Western blot with the indicated primary antibodies (1:800–1:8,000) and their corresponding secondary antibodies. Signal acquisition was performed with chemiluminescent HRP substrate (Millipore), and the results were imaged with an FX5s system (Vilber Lourmat). ImageJ was used for quantitative analysis of the gray values.

In Vitro Wounding Healing Assay and Cell Migration Assay

The in vitro wound healing assays were performed as previously described (16,24). Briefly, cells (150,000 cells/mL) were seeded into a 35-mm well, in which an ultraviolet-sterilized polydimethylsiloxane (PDMS) strip (1 mm × 2 cm) was

transversally placed in the middle of the well bottom. After cell monolayers formed, the PDMS strips were removed to generate gaps, and cells were treated with the indicated compounds until the wounds were almost closed. To assess the cell migration ability in vitro, we performed transwell migration assays in 24-well invasion chambers. Cells were plated in the top chamber with 200 μL serum-free medium, and 600 μL medium supplemented with 20% FBS was used as a chemoattractant in the bottom chamber. As previously described, the cells were given 24 h to migrate, after which the cells were fixed and stained with crystal violet. Counts were made from 10 randomly chosen separated fields (original magnification ×10) (12).

Cell Proliferation Assay and Small Interfering RNA Transfection

For cell proliferation assays, HaCaT cells (1,000 cells/well) or HFFs (2,000 cells/well) were seeded into 96-well plates and incubated with Sax (10 μmol/L) and Sit (100 μmol/L) for 0, 24, 48, 72, and 96 h. Subsequently, 100 μL fresh medium containing 10 μL Cell Counting Kit 8 (CCK8) solution (Dojindo Molecular Technologies) was added to each well and incubated for 40 min at 37°C in 5% CO_2. The cell growth curves were acquired with CCK8 using a Varioskan Flash microplate reader (Thermo Scientific) at an absorbance of 450 nm. For small interfering (si)RNA transfection, HaCaT cells were transfected with a control siRNA (Con siRNA; Qiagen) or a NRF2-specific siRNA (Qiagen) (Supplementary Table 2) using the HiPerFect Transfection Reagent (Qiagen) according to the manufacturer's instructions. Cells were transfected with siRNA for 72 h and harvested for Western blot. In the in vitro wound healing assays, the PDMS strips were moved at 48 h of siRNA transfection, and cells were allowed to migrate.

DPP-4 Activity Assay

To assess tissue DPP-4 activity, a commercial DPP-4 Activity Assay Kit for tissues or cells (#K779-100, BioVision) was used, following the manufacturer's instructions (12); in this kit, DPP-4 cleaves a substrate to release a quenched fluorescent group, 7-amino-4-methyl coumarin (AMC). In detail, 10 mg tissue was homogenized in 150 μL DPP-4 assay buffer on ice and centrifuged at 13,000*g* for 10 min at 4°C to remove insoluble material. Prepared duplicate samples (one for background control and one for sample testing) were added (up to 50 μL/well) to a 96-well black plate. For the background control, 10 μL DPP-4 assay buffer was added to one sample replicate, and 10 μL DPP-4 inhibitor was added to another sample as the sample background control. The samples were incubated for 10 min at 37°C, and 40 μL reaction mix (DPP-4 assay buffer and DPP-4 substrate) was added to each well, mixed well, and incubated at 37°C while shielded from light. The fluorometric values (360 nm excitation; 460 nm emission) of the samples (S) and background controls (B) were read with a Varioskan Flash microplate reader during the reaction at 37°C. To calculate the sample activity, the relative fluorescence unit (RFU) of fluorescence generated by substrate cleavage of by DPP-4 was computed as $\Delta RFU = (R_{S2} - R_{B2}) - (R_{S1} - R_{B1})$. After plotting the AMC standard curve, ΔRFU was applied to the standard curve to obtain the AMC amount (pmol): Activity = AMC amount/$[(T_2 - T_1) \times V] \times$ sample dilution factor = pmol/min/mL = μU/mL. $(T_2 - T_1)$ is the interval between two readings (in min), and V is the sample volume added into the reaction well (in mL). One unit is defined as the amount of DPP-4 that hydrolyzes the DPP-4 substrate to yield 1.0 μmol of AMC per min at 37°C.

Hematoxylin and Eosin, Masson Trichrome, and IHC Staining

Human and mouse skin tissues were fixed in 4% paraformaldehyde (Boster) overnight and washed for 1 h before being dehydrated and embedded in paraffin. Then, 3.5 μm tissue sections were prepared for hematoxylin and eosin (H&E), Masson trichrome staining (Sigma-Aldrich), and IHC staining according to the standard protocol. Samples underwent standard deparaffinization, rehydration, and antigen retrieval (sodium citrate buffer, pH 6.0) for IHC staining of tissues, performed as described previously. As a negative control, primary antibodies were replaced with class-matched IgG isotypes, and staining was performed using standard 3,3′-diaminobenzidine chromogen detection. IHC staining was scored independently by two pathologists for percentage of positive cells (five categories: 0 [<10%], 1 [10–25%], 2 [25–50%], 3 [50–75%], and 4 [75–100%]) and intensity (four categories [from low to high]: 0, 1, 2, and 3). A final IHC staining score (intensity score × percentage score) was determined.

Immunofluorescence

Human and mouse wound skin tissues embedded in optimal cutting temperature compound were cut into 3.5-μm sections and fixed with 100% methanol at −20°C for 20 min, and cell slides were fixed with 4% paraformaldehyde at room temperature for 15 min. Tissue sections were permeabilized with 0.2% Triton-X 100 for 5 min, and the cell slides were incubated in ice-cold methanol for 2 min. Next, these specimens were incubated with 5% BSA for 30 min at room temperature to block nonspecific binding, incubated with the indicated primary antibodies at 4°C overnight, and then incubated with the corresponding secondary antibodies at room temperature for 1 h. Subsequently, 100 μL DAPI (Beytime C1006) was applied for 10 min at room temperature to stain cell nuclei. Finally, the specimens were mounted on coverslips with (10–20 μL) drops of Fluoromount (Boster), and the fluorescence images were obtained using a TC5-SP5 confocal laser scanning microscope (Leica).

Experimental Animals and Protocols

Experimental *Nrf2*$^{+/+}$ and *Nrf2*$^{-/-}$ C57BL/6 male mice were purchased from the Model Animal Research Center of Nanjing University and were housed and handled according to the Third Military Medical University Institutional Animal Care policies. The diabetic wound animal model was described previously (16). Briefly, 10-week-old mice were administered a 50 mg/kg streptozotocin (STZ) injection for 5 consecutive

days. After 5 weeks, mice with fasting glucose levels >250 mg/dL (Roche) were considered diabetic and were randomly allocated to the indicated treatment groups. Mice received 15 mg/kg Sax or an equivalent amount of normal saline (vehicle [Veh]) via intragastric administration daily until the end of the experiment. One week after Sax/Veh treatment, mice were anesthetized with inhaled 2% isoflurane, and two wounds were made on the back of each mouse with a sterile 6-mm skin biopsy punch (HealthLink).

To observe the continuous effect of DPP-4i treatment on skin wound areas, wounds of diabetic mice were monitored using a digital camera with the same ruler at day 0 and every other day. After the wound images were collected, the size of each wound area was quantified with a unified calibration using the ImageJ software. Wound closure was calculated as the percentage of the original wound area that had healed at the indicated time points (wound closure rate = [1 − (wound area day *x*/wound area day 0)] × 100%). Mice were sacrificed by cervical dislocation at days 4, 7, 11, and 14 after surgery, and wound tissues were harvested using an 8-mm skin biopsy punch (n = 5–6 mice/group per time point).

Clinical Study

This clinical trial (ClinicalTrials.gov NCT02742233) was performed under strict compliance with the institutionally approved guidelines by the Xinqiao Hospital Ethics Committee, Third Military Medical University of People's Liberation Army, China. All participants gave their written informed consent before being enrolled. The flowchart of patient screening and enrollment is presented in Fig. 6.

This study enrolled male and female subjects diagnosed with T2D who were 45 to 85 years of age with Wagner grade 2–4 ulcers located in the lower extremities. Subjects were determined to be ineligible if they had severe organ failure (liver, heart, or kidney), uncontrolled diabetes with acute complications, serious ulcer infection or nondiabetic ulcers (orthopedic or neuromuscular pathological conditions), history of malignancy, or pregnant or breast-feeding women. The enrolled subjects were randomly divided into the placebo and Sax groups: regular treatment (insulin and some other oral hypoglycemic agent) without or with Sax (5 mg, per os, q.d.). Human perilesional skin tissue samples surrounding the wounds (margin within 1 cm) were collected after 1 week of placebo or Sax treatment. The subjects were monitored for 13 weeks to evaluate the ulcer outcome.

Statistical Analysis

The results are expressed as the mean ± SD, the median and range, or the absolute and percentage frequencies. Statistical tests were performed using GraphPad Prism 6.0 and SPSS 23.0 software. Comparisons between two data sets of continuous variables were assessed with the Student t test, and ANOVA was used to analyze three or more than three data sets. The Wilcoxon rank sum test (Mann-Whitney) was used to analyze the IHC scores. The χ^2 test for proportion of categorical variables was performed to compare certain characteristics of the participants, including healed ulcers, new ulcers, recurrent ulcers, amputation, sex, Wagner classification, ulcer location, diabetic complication, comorbidities, and therapy. Kaplan-Meier analysis was used to evaluate the median time to complete wound closure. For evaluating the clinical outcome, the clinical data were assessed using an intention-to-treat approach. $P < 0.05$ was considered statistically significant.

RESULTS

DPP-4i Accelerates Diabetic Wound Healing In Vitro and in STZ-Induced Mice

To assess the effect of DPP-4i on diabetic wound healing, we first performed a wound healing assay in vitro using a human keratinocyte cell line. Compared with the control group, a clear reduction in wound area was observed upon treatment with a range of different DPP-4is (commercial human drugs Sax, Sit, Alo, Vil, and Lin) at each of the time points indicated (Fig. 1*A* and *B*). Because there were no statistically significant differences in the wound healing effects among the different DPP-4is, we selected Sax as a representative DPP-4i for further experiments.

To confirm the positive wound-healing effects of DPP-4i treatment, we observed the wound closure rate in mice with STZ-induced diabetes (Fig. 1*C*). Consistent with our in vitro results, 15 mg/kg Sax treatment significantly accelerated the diabetic wound closure rate over the course of the healing process ($P < 0.001$) (Fig. 1*D* and *E*). Moreover, the pathological morphology and diameters of cutaneous wounds on the day 14 postsurgery were assessed with H&E staining, which showed a more mature histological appearance and shorter diameter of wounds in the Sax-treated mice and further confirmed the effective amelioration of diabetic wound healing (Fig. 1*F*). Taken together, these results indicated that DPP-4i treatment improves diabetic wound healing in vitro and in vivo.

DPP-4i Promotion of Diabetic Wound Healing Is Not Primarily Mediated Through the NRF2 Pathway

Previous reports have shown that DPP-4i can activate NRF2 (12,13) and that the NRF2 pathway plays a protective role in diabetic ulcers (DUs) (16,17). Thus, we next sought to determine whether the improved diabetic wound healing under DPP-4i treatment was mediated through NRF2. In vitro experiments showed that NRF2 knockdown delayed wound healing (NRF2 siRNA vs. Con siRNA group without Sax, P = 0.0014), which is consistent with our previous observations (16). However, Sax was still effective in reducing the size of wound areas under NRF2 knockdown conditions (NRF2 siRNA without Sax vs. NRF2 siRNA with Sax, $P < 0.05$), and the decrease in gradients was not significantly different compared with Con siRNA conditions (Δ relative wound area %: Con siRNA vs. NRF2 siRNA) (Supplementary Fig. 1*A*). Moreover, the in vivo experiment showed that Sax maintained its ability to promote diabetic wound closure in $Nrf2^{-/-}$ mice (P = 0.007) (Supplementary Fig. 1*B*). Collectively, these results indicated that NRF2 is not the major mechanism by which the effect of DPP-4i on diabetic wound healing is mediated.

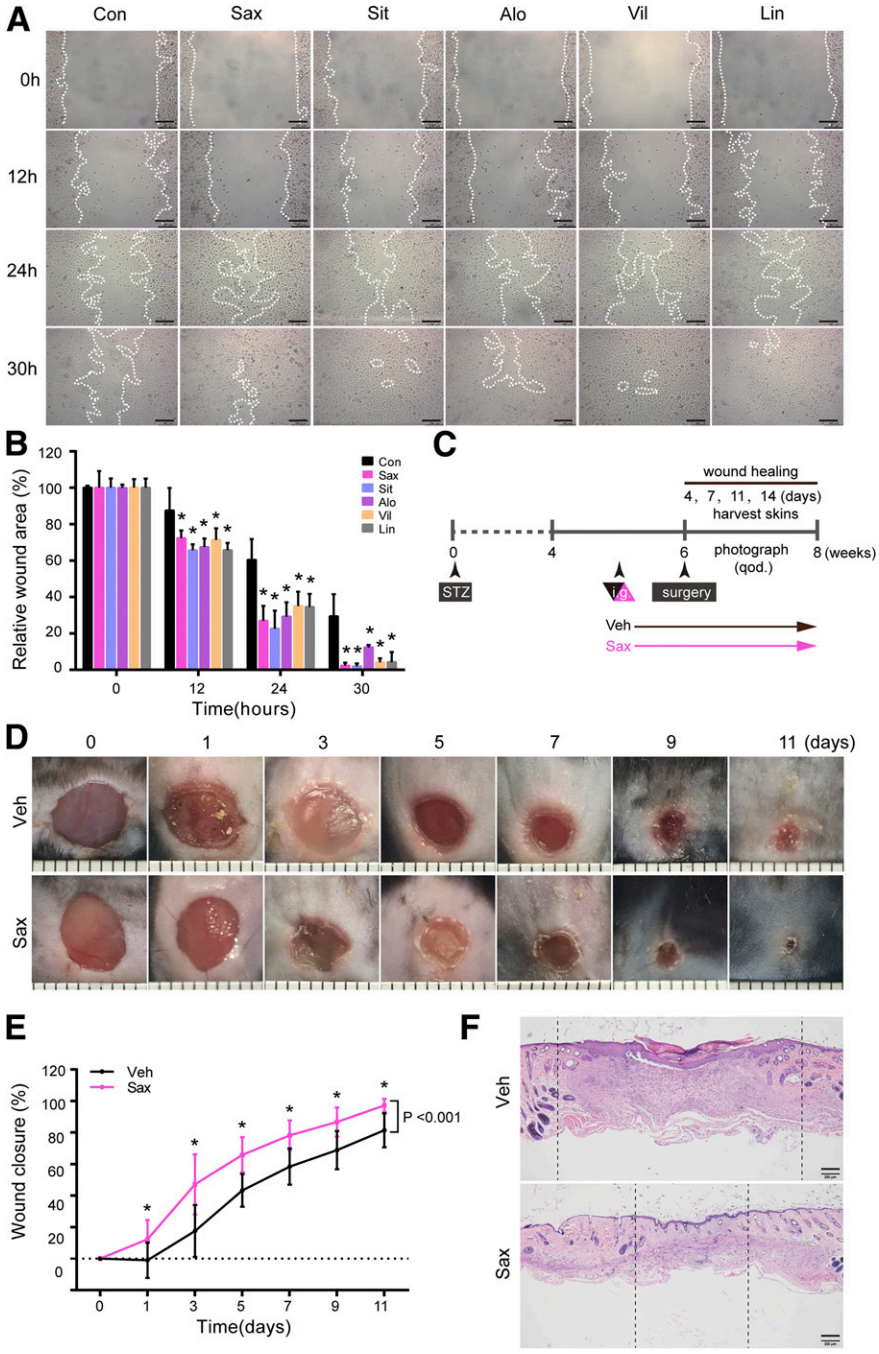

Figure 1—DPP-4i accelerates diabetic wound healing in vitro and in STZ-induced mice. *A* and *B*: In vitro wound healing assay of keratinocytes. After monolayers formed in HaCaT cells, the preplaced PDMS strips were removed to generate gaps, and HaCaT cells were treated with DPP-4is (10 μmol/L Sax, 100 μmol/L Sit, 40 μmol/L Vil, 40 μmol/L Alo, or 20 μmol/L Lin) for up to 30 h. *A*: Representative images of each group at the indicated time points after gap formation are shown. The white dotted lines represent the wound boundary. Scale bar, 100 μm. *B*: The wound area percentage is shown. The results are expressed as the mean ± SD; $n = 4$. *$P < 0.05$ (as analyzed by ANOVA). *C*: The timelines of animal studies are shown. A diabetic mouse model was established through five consecutive intraperitoneal STZ injections. Five weeks later, mice with fasting glucose levels ≥250 mg/dL were selected for use as diabetic models. These diabetic mice were randomly allocated into Veh or Sax groups and received normal saline or 15 mg/kg Sax daily, respectively, until the end of the experiment. Operations to create wounds were performed after 1 week of drug treatments, with two wounds being made on back of each mouse. After surgery, wounds were monitored via digital imaging. Mice (n = 5–6 per group) were sacrificed, and the skin tissues were harvested at days 4, 7, 11, and 14. *D–F*: To observe the wound areas, the wounds were photographed at day 0 and every other day after surgery; mice were sacrificed at day 14 after surgery. *D*: The representative images of wounds in each group at the indicated time points are shown. *E*: The wound areas were measured, and wound closures (the percentage of wound that healed) were calculated at the indicated time points (n = 10–12). The results are expressed as the mean ± SD. *$P < 0.05$ as determined by ANONA and the Student t test. *F*: The pathological morphology and the diameter of cutaneous wounds in each group were assessed with H&E staining. The borders of the wounds are indicated by black dotted lines. Scale bar, 200 μm. Con, control, equivalent dose of DMSO.

DPP-4i Induces EMT of Keratinocytes

We next explored other possible mechanisms behind the amelioration observed. We chose to focus on keratinocytes and fibroblasts because these two types of cells are known to play critical roles in wound healing (25–27) and both are the major sources of DPP-4 in the skin (28). Our data showed that DPP-4is (Sax and Sit) did not affect the proliferation of keratinocytes (HaCaT cells) (Supplementary Fig. 2*A*) and HFFs (Supplementary Fig. 2*B*) as assessed by CCK8, or alter the migration of HFFs detected with a transwell assay (Supplementary Fig. 2*C*). However, DPP-4is promoted the migration of keratinocytes (Fig. 1*A*). Intriguingly, keratinocytes showed EMT-like morphological changes (shifting from a cuboidal epithelial phenotype into a more

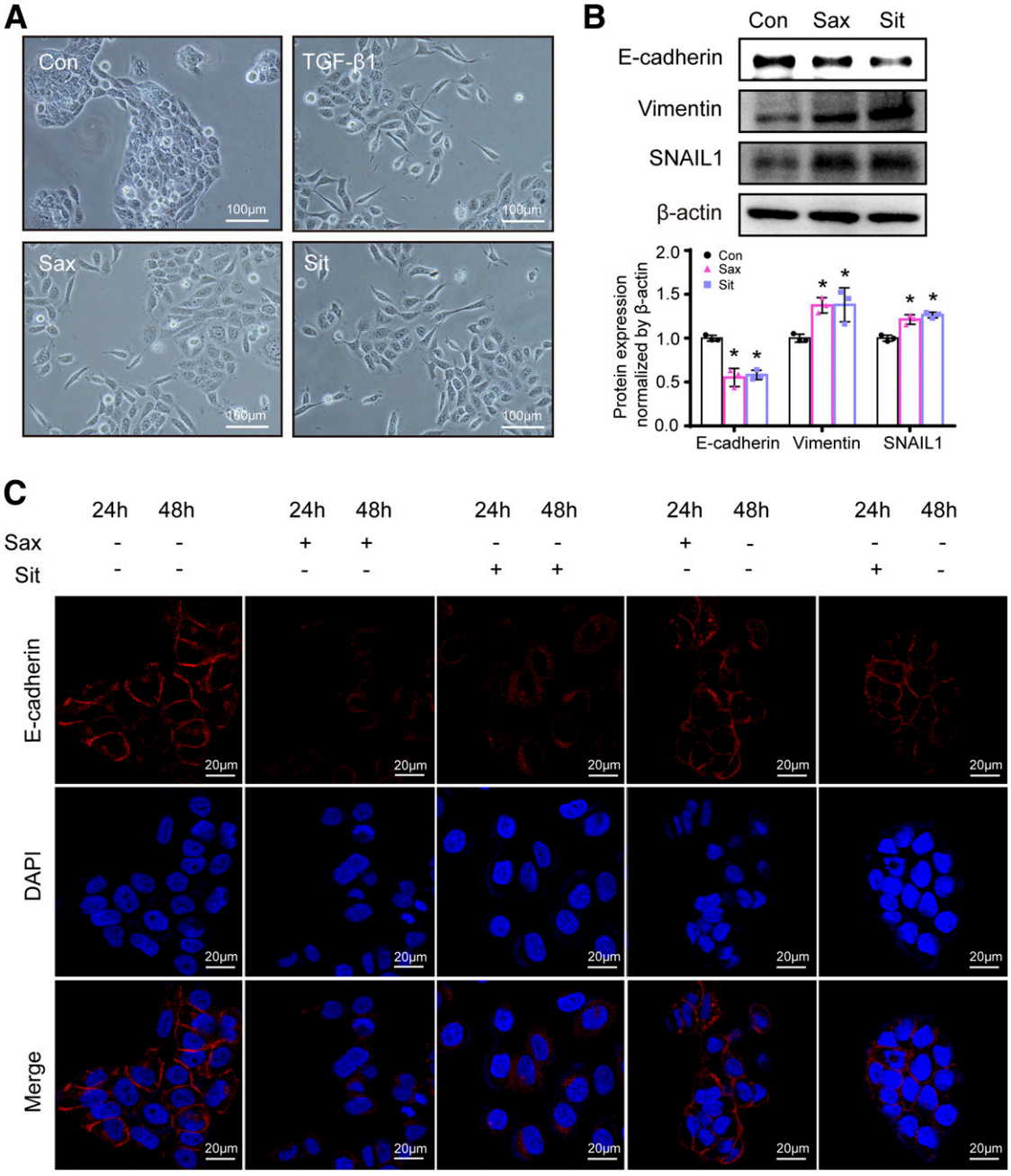

Figure 2—DPP-4i induces EMT of keratinocytes directly. *A* and *B*: HaCaT cells were treated with compounds 10 μmol/L Sax, 100 μmol/L Sit, or 5 ng/mL TGF-β1 for 24 h. *A*: Cell morphology was assessed under a phase contrast microscope. Scale bar, 100 μm. *B*: The expression levels of EMT-associated proteins (E-cadherin, vimentin, and SNAIL1) were detected by Western blot and quantified. Results are presented as the mean ± SD, $n = 3$. *$P < 0.05$ as determined by ANOVA. *C*: HaCaT cells were incubated with DPP-4i compounds (10 μmol/L Sax or 100 μmol/L Sit) for 24 h and then switched to fresh medium with or without DPP-4i for another 24 h. Representative immunofluorescence images of the indicated antibody (anti-E-cadherin, red) and DAPI (blue) nuclear staining are shown. Scale bar, 20 μm. Con, control, equivalent dose of DMSO.

elongated shape that is typical of mesenchymal cells) after Sax and Sit treatment, which was similar to the alterations induced by TGF-β1 (Fig. 2*A*). This phenomenon was also replicated using three other DPP-4is (i.e., Alo, Vil, and Lin) (Supplementary Fig. 3*A*).

Based on those observations and given that EMT is an important mechanism for keratinocytes migration (27,29), we then investigated the effects of DPP-4i on EMT. Western blot for key EMT-associated proteins showed that DPP-4i reduced E-cadherin expression while increasing the expression of vimentin and SNAIL1 (Fig. 2*B* and Supplementary Fig. 3*B*). The morphological changes and decreased expression of E-cadherin were further confirmed through immunofluorescence (Fig. 2*C*, left three lines). To address the association between DPP-4i treatment and EMT induction, Sax and Sit were removed after 24 h. Immunofluorescence showed that compared with 48 h of continuous DPP-4i treatment, the expression and location of E-cadherin, as well

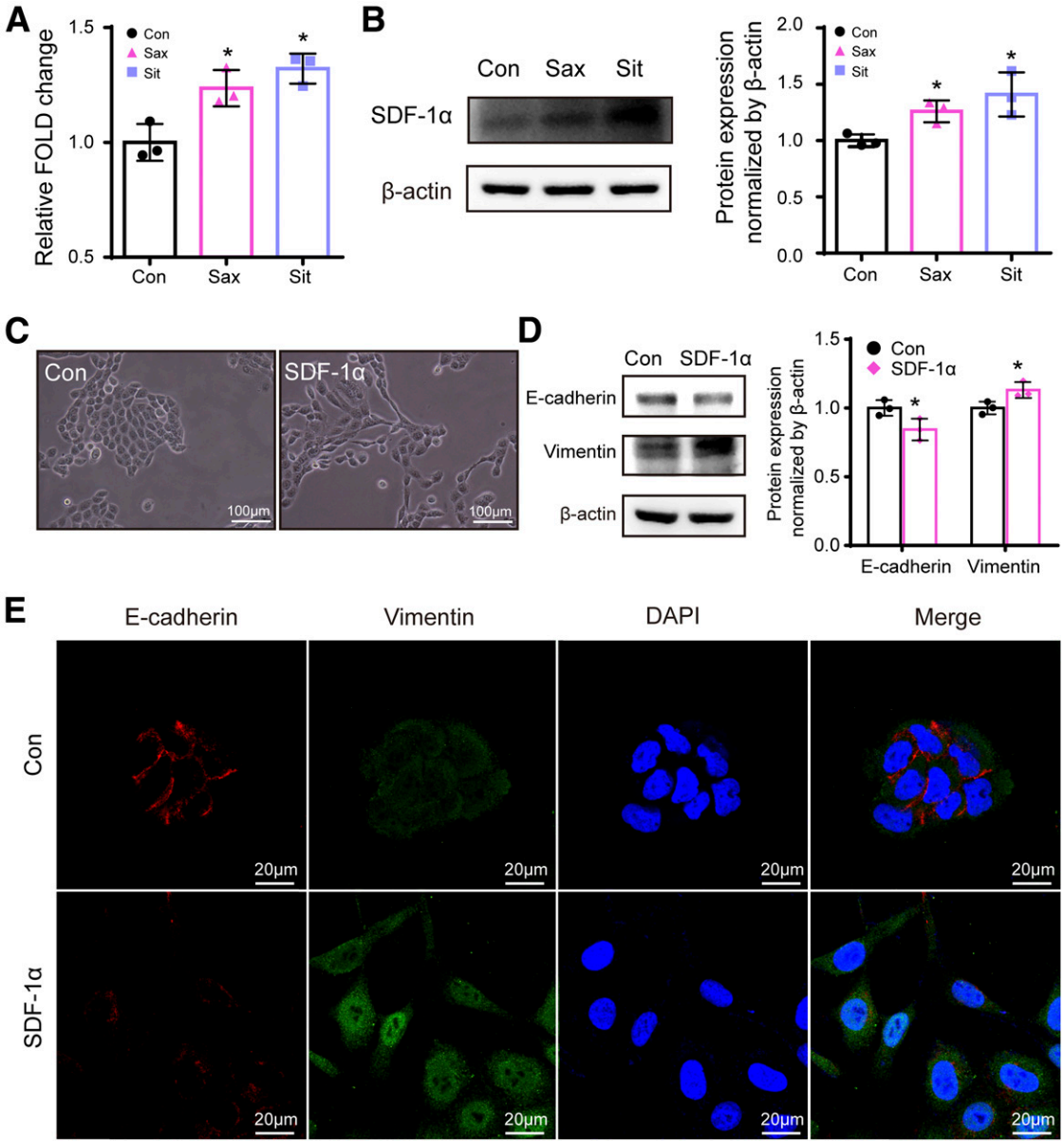

Figure 3—DPP-4i promotes SDF-1α production of fibroblasts driving keratinocytes EMT indirectly. *A* and *B*: HFFs were treated with compounds 10 μmol/L Sax or 100 μmol/L Sit for 24 h. *A*: Total RNAs was extracted, and qRT-PCR was performed to measure the mRNA levels of SDF-1α in HFFs. *B*: The SDF-1α protein levels of HFFs treated with DPP-4i were assessed by Western blot and quantified. Results in *A* and *B* are presented as the mean ± SD, $n = 3$. *$P < 0.05$ as determined by ANOVA. *C–E*: HaCaT cells were treated with 150 ng/mL SDF-1α for 24 h. *C*: Cell morphology was assessed under a phase contrast microscope. Scale bars, 100 μm. *D*: Cell lysates were subjected to Western blot for EMT-associated proteins (E-cadherin and vimentin), and the expression levels were quantified. Results are presented as the mean ± SD, $n = 3$. *$P < 0.05$ as determined by the Student *t* test. *E*: HaCaT cells were assessed by immunofluorescence (E-cadherin, red; vimentin, green; DAPI, blue) under a laser microscope, and representative images are shown. Scale bar, 20 μm. Con, control, equivalent dose of DMSO.

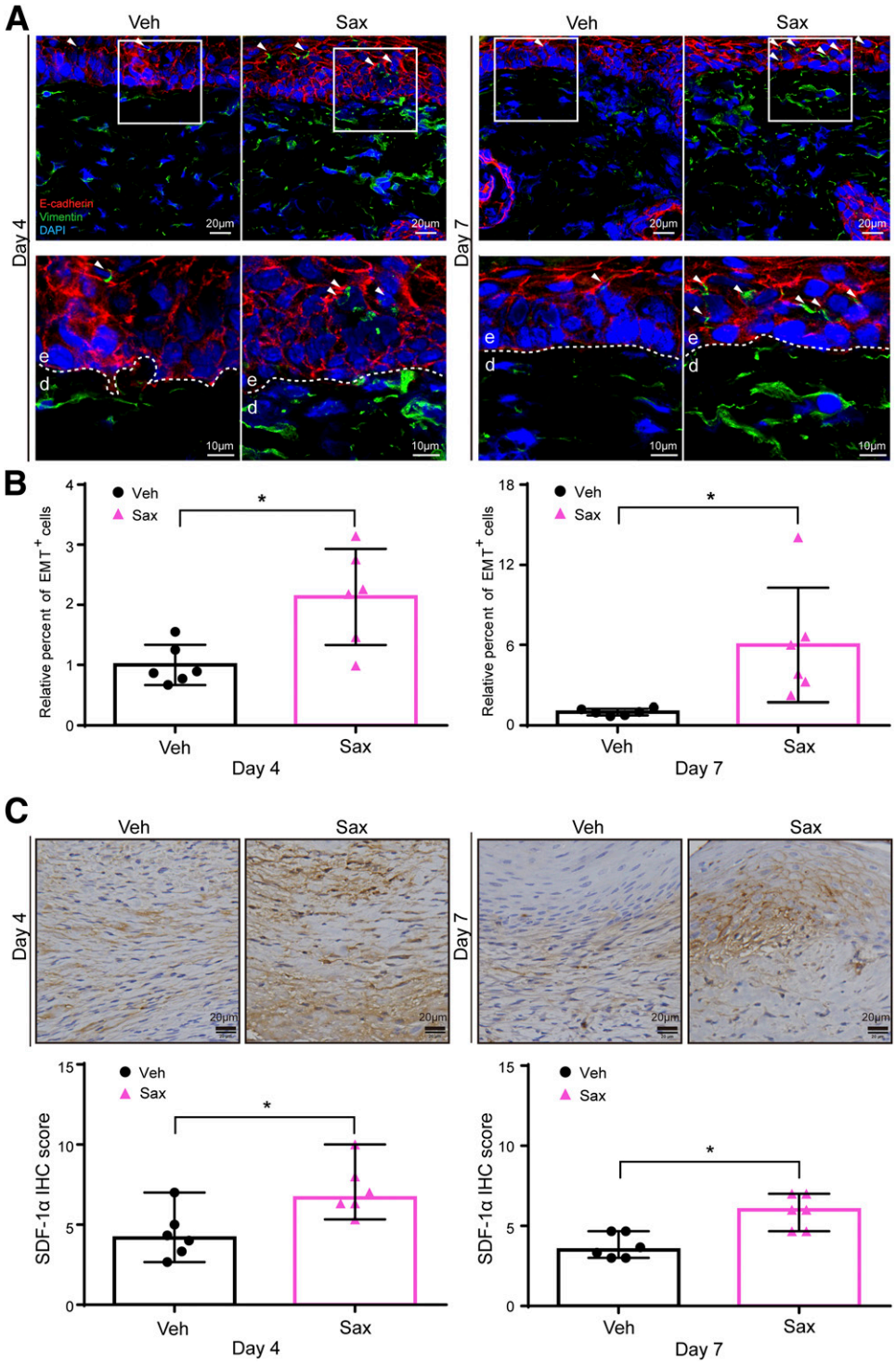

Figure 4—DPP-4i induces EMT and SDF-1α expression in diabetic mice. *A* and *C*: To detect EMT, as described in Fig. 1*C*, mice were sacrificed and the wound skin tissues were harvested at days 4 and 7 postsurgery. Immunofluorescence was performed to assess the expression and localization of EMT-associated proteins, and the shift to mesenchymal features by the epithelial cells at the deep ridges of epidermis layer can be seen by their vimentin expression. *A*: Representative images of skin sections (E-cadherin, red; vimentin, green; DAPI, blue) are shown at low magnification (original magnification ×800, upper panel) and high magnification (original magnification ×2,000, lower panel). e, epidermis layer; d, dermis layer; dashed white line, epidermal-dermal boundary; white arrows, EMT^+ cells. Scale bars, 20 μm and 10 μm. *B*: The numbers of EMT^+ cells and total epithelial cells were counted, and the relative percentage of EMT^+ cells is shown. The results are expressed as the mean ± SD, n = 6 mice. *$P < 0.05$ as determined by the Student t test. *C*: The expression of SDF-1α protein in mouse wound skin tissues was detected by IHC. Representative IHC images and quantification results are shown. Scale bars, 20 μm. The results are expressed as the median and range, n = 6 mice. *$P < 0.05$ as determined by Mann-Whitney test.

as the polarity and morphology of HaCaT cells, were restored after 24 h DPP-4i withdrawal (Fig. 2*C*, right two lines), which is similar to the basal level (without DPP-4i treatment) (Fig. 2*C*, left first line). Overall, these results suggested that DPP-4i induced keratinocyte migration through EMT.

DPP-4i Promotes SDF-1α Production of Fibroblasts Indirectly Driving Keratinocytes EMT

Fibroblasts are another vital cell type in skin repair in addition to keratinocytes. Although DPP-4i did not affect fibroblast proliferation and migration (Supplementary Fig. 2*B* and *C*), previous studies have identified a number of fibroblast-secreted cytokines that also play important roles in cutaneous wound healing, such as VEGF (30), TGF-β1 (31), SDF-1α (CXCL12) (32), COX-2 (33), and HMGB1 (34) etc. Next, we preliminarily screened these cytokines via Western blot, and our data showed that compared with the Con group, DPP-4i treatment did not affect the protein expression levels of VEGF, TGF-β1, COX-2, or HMGB1 (Supplementary Fig. 4) but increased the mRNA and protein levels of SDF-1α in fibroblasts as detected by qRT-PCR and Western blot, respectively (Fig. 3*A* and *B*). Because recent studies have shown that SDF-1α secreted from cancer-associated stromal cells promotes migration of multiple cancer cell types by inducing EMT (35,36), we then tested whether SDF-1α derived from fibroblasts can also promote EMT of keratinocytes. Our data showed that compared with the Con group, SDF-1α treatment indeed led to changes in keratinocytes from epithelial to fibroblast-like morphology (Fig. 3*C*), accompanied with downregulation of E-cadherin and upregulation of vimentin expression ($P < 0.05$) (Fig. 3*D*). Immunofluorescence further confirmed that SDF-1α treatment resulted in the transition of keratinocytes into a mesenchymal phenotype and in altered levels of EMT-associated proteins (downregulated E-cadherin and upregulated vimentin) compared with the Con group (Fig. 3*E*). These results demonstrated that DPP-4i can also indirectly promote keratinocyte EMT via enhanced SDF-1α expression of fibroblasts.

DPP-4i Induces SDF-1α Expression and EMT in Diabetic Mice

To confirm the mechanisms observed in vitro, we attempted to replicate the results in vivo. Our data showed that compared with those of diabetic mice without DPP-4i treatment (Veh group), the DPP-4 activities of DPP-4i–treated diabetic mice (Sax group) were obviously lower in the skin wound edges (Supplementary Fig. 5*A*). At the same time, DPP-4i treatment had no influence on body weight (Supplementary Fig. 5*B*) or blood glucose (Supplementary Fig. 5*C*), indicating that the effect of DPP-4i in promoting diabetic wound repair is independent of glycemic control. Immunofluorescence analysis of tissues revealed that the

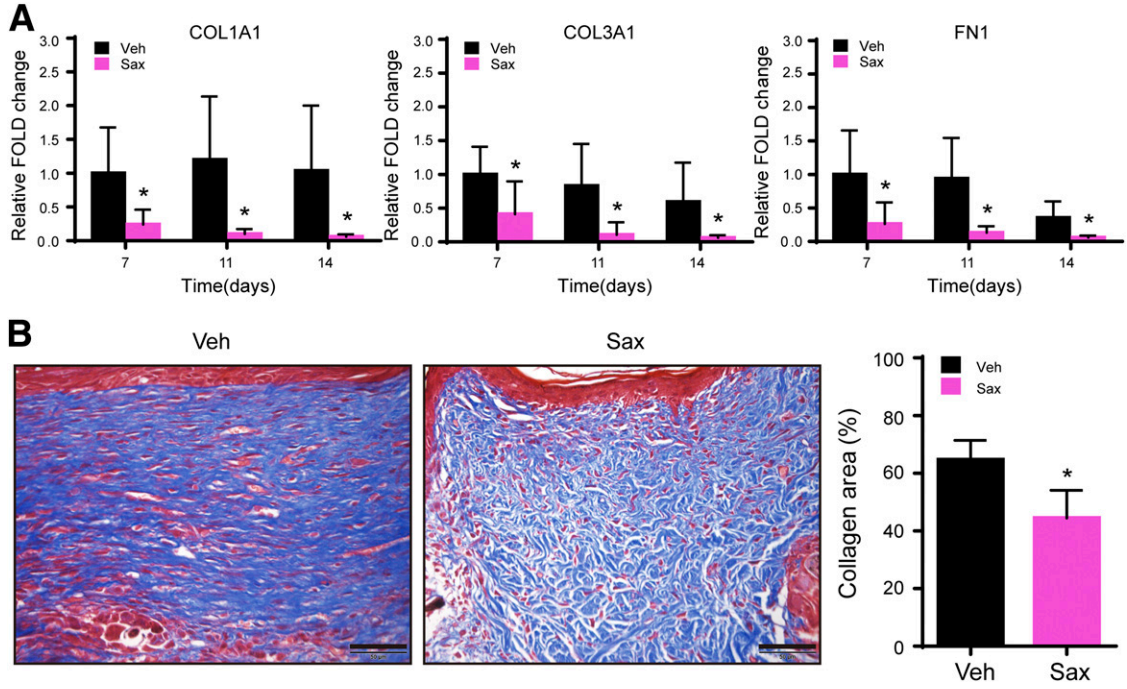

Figure 5—DPP-4i attenuates scar formation in STZ-induced diabetic mice. *A* and *B*: To assess scarring, as described in Fig. 1*C*, the mouse wound skin tissues were harvested at days 7, 11, and 14 postsurgery. *A*: Total mRNA of tissues was analyzed with qRT-PCR to detect the mRNA transcripts of COL1A1, COL3A1, and FN1. The relative mRNA levels are shown. The results are expressed as the mean ± SD, $n = 6$. *$P < 0.05$ compared with Veh, as determined by the Student *t* test. *B*: Masson trichrome staining was used to detect the collagen area (blue) of wound tissues on day 14 after surgery. Representative images (left panel) and relative collagen areas (right panel) are shown, Scale bars, 50 μm. The results are expressed as the mean ± SD, $n = 18$. *$P < 0.05$ as determined by the Student *t* test.

Sax group had a larger number of epithelial cells undergoing EMT at the wound sites, with a particularly notable increase of vimentin-expressing cells localized in the epithelial layer (green, indicated by white arrow) during the proliferation phase (Fig. 4*A*). Morphometric analysis showed that the Sax group had an approximately two- to sixfold larger EMT-positive cell population than did the Veh group (Fig. 4*B*). Moreover, significantly increased levels of SDF-1α were detected by IHC in the wound tissues of Sax-treated mice ($P < 0.05$) (Fig. 4*C*). The changes in the expression of EMT-associated proteins and SDF-1α during the wound healing process were also confirmed by Western blot (Supplementary Fig. 6*A* and *B*). Taken together, these in vivo data further confirmed that DPP-4i improves diabetic wounds through inducing keratinocyte EMT.

DPP-4i Attenuates Scar Formation of Diabetic Wounds in Mice

Recent studies have shown that DPP-4 activity may be involved in scar formation (37,38). Thus, we subsequently assessed the effect of DPP-4i at the remodeling phase in diabetic mice. Pathological scar formation is typically associated with excessive extracellular matrix (ECM) deposition (26,38,39). Our data showed that compared with the Veh group, the Sax group had lower levels of major ECM-related genes (COL1A1, COL3A1, and FN1), which indicated that DPP-4i treatment reduced the synthesis of ECM during the remodeling phase in the cutaneous wound tissue of diabetic mice (Fig. 5*A*). Accordingly, the Sax group showed more mature organization and less collagen deposition than the Veh group, detected by Masson trichrome staining (Fig. 5*B*). Collectively, these findings indicated that DPP-4i can diminish scar formation by attenuating ECM deposition.

DPP-4i Improves Wound Healing in Patients With T2D

Having observed the efficacy of DPP-4i treatment in promoting wound healing in vitro and in vivo and gained some insight into the mechanisms involved, we then sought to characterize the clinical application of DPP-4i in treating DUs in patients with T2D. A clinical trial (NCT02742233) consisting of 67 patients with T2D with DUs was conducted. The participant flow through the trial is shown in Fig. 6. Briefly, 74 participants were screened and 7 were excluded, with 35 participants in the placebo group and 32 in the Sax group. The characteristics of the enrolled participants are presented in Supplementary Table 1. The baseline profile of both groups was similar with regard to demographics (age, BMI, sex, etc.), characteristics of T2D (diabetes duration, complications, therapy, blood glucose, etc.), and ulcers (Wagner classification, ulcer area, ulcer location, etc.). No differences were found in HbA_{1c} and blood glucose levels after treatment (Supplementary Table 1). However, compared with baseline, the DPP-4 activity in the perilesional wound tissues of the Sax group obviously decreased after treatment (Supplementary Fig. 7). A significant improvement in the healed ulcer rate and time for complete wound closure was observed in the Sax-treated

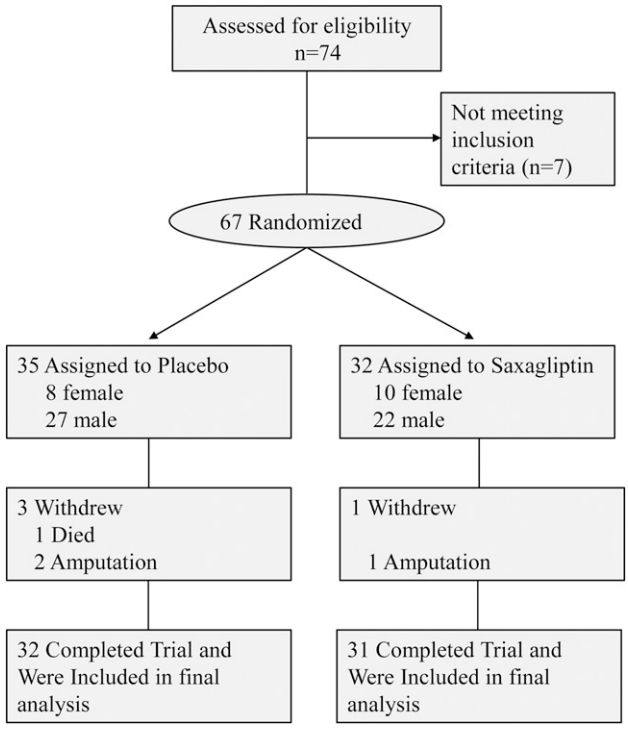

Figure 6—Participant flow through the trial. In total, 74 participants were screened, 7 were excluded, and 67 met the eligibility criteria and were enrolled in the randomized controlled trial: 35 participants in the placebo group and 32 participants in the Sax group.

group (Table 1). In addition, a Kaplan-Meier curve (log-rank = 15.08, $P = 0.0001$) further confirmed that DPP-4i increased the rate of wound healing assessed at different time points (Fig. 7*A*). Moreover, consistent with our in vitro and animal data, the Sax-treated group showed a larger number of cells undergoing EMT (Fig. 7*B*) and higher SDF-1α expression levels than the placebo group (Fig. 7*C*). These clinical data further confirmed the effects of DPP-4i on diabetic wound healing. Collectively, our results indicated that DPP-4i accelerated diabetic wound healing through improving the functions of keratinocytes and fibroblasts at different phases of the wound repair process (Fig. 8).

Table 1—Outcome achieved according to DPP-4i treatment in patients with diabetes with ulcers

Outcomes	Placebo (n = 35)	Sax (n = 32)	P value
Healed ulcers	18 (51.42)	28 (87.50)	0.001
Time to complete wound closure, days	88 (63–91)	73 (47–91)	<0.001
New ulcers	2 (5.71)	2 (6.25)	0.658
Recurrent ulcers	2 (5.71)	1 (3.13)	0.534
Amputation	2 (5.71)	1 (3.13)	0.534

Data are shown as n (%) or median (range). Reported at the 13th week over the follow-up period.

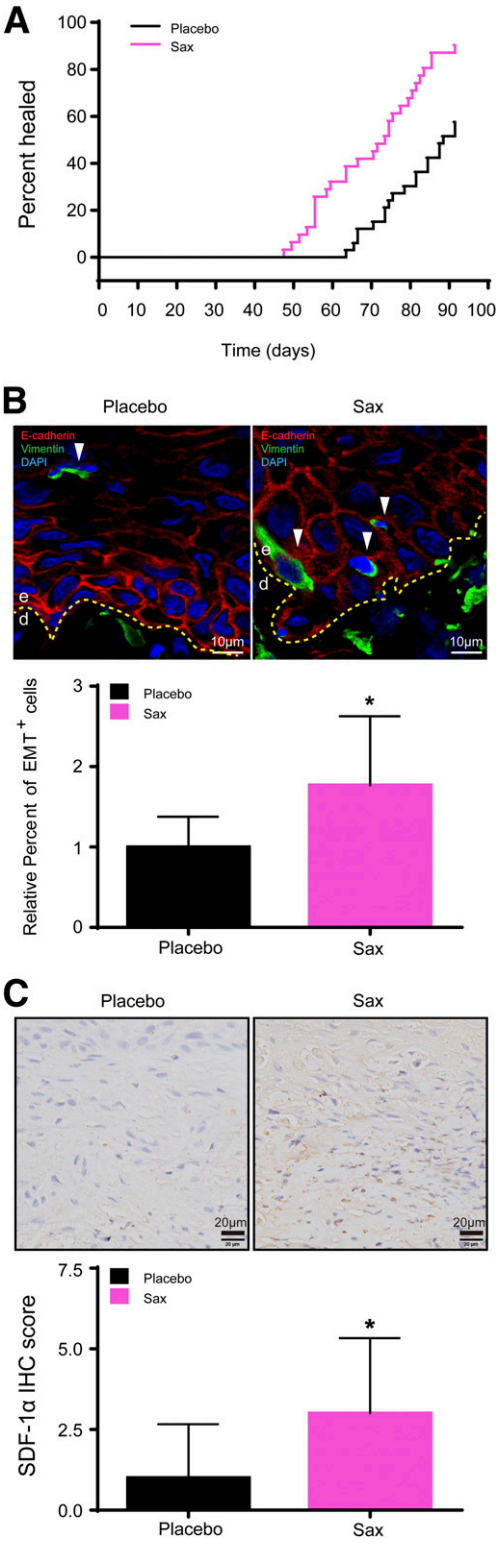

Figure 7—DPP-4i improves wound healing in patients with diabetes. *A–C*: As described in the RESEARCH DESIGN AND METHODS, patients with diabetes with ulcers were randomly divided into the placebo (n = 35) or Sax (n = 32) groups for 13 weeks of follow-up. *A*: Kaplan-Meier estimates of accumulated ulcer healing events up from zero. Log rank = 15.08, P = 0.0001 relative to the placebo-treated group. *B*: Perilesional skin tissue samples surrounding the wound of the patients were collected after 1 week of treatment. Immunofluorescence detected the expression and localization of EMT-associated proteins (E-cadherin, red; vimentin, green). EMT^+ epithelial cells of the epidermis layer are demonstrated by vimentin expression (DAPI, blue). Representative images are shown (original magnification ×2,000, upper panel). e, epidermis layer; d, dermis layer; dashed yellow line, epidermal-dermal boundary; white arrows, EMT^+ epithelial cells. Scale bars, 10 μm. The relative percentage of EMT^+ cells is shown in the lower panel. The results are expressed as the mean ± SD, n = 18. *$P < 0.05$ as determined by the Student t test. *C*: The expression of SDF-1α protein in human wound skin tissues was detected by IHC. Representative images and quantification results are shown. Scale bars, 20 μm. *$P < 0.05$ as determined by Mann-Whitney test.

DISCUSSION

DPP-4 activity and protein levels have been shown to fluctuate during wound healing under physiological conditions, and DPP-4 knockout mice displayed faster wound healing capabilities (22), suggesting that DPP-4 might act to inhibit the rate of normal regeneration. However, there are limited data on the role of DPP-4 in impaired wound healing processes under pathological conditions, such as diabetes. Here, we demonstrated that a class of common clinical hypoglycemic drugs, DPP-4is, accelerates diabetic wound healing through multiple mechanisms during different phases, which indicates that DPP-4 is also involved in the pathological wound healing process. Previous studies have revealed some other additional effects of DPP-4i, such as alleviation of kidney fibrosis (10), antiatherosclerotic effects (11), and tumor metastasis promotion (12,13). All of these findings may influence the strategy for clinical application of DPP-4i in the future.

Optimum healing of cutaneous wound requires a well-orchestrated integration of the complex biological functions of multiple cells (27,40). Our study revealed that DPP-4i coordinated the cellular activities of keratinocytes and fibroblasts to induce EMT. EMT has been well established as being an essential process to accomplish reepithelialization in wound repair (41), and our data showed that DPP-4i treatment was sufficient to directly trigger EMT of keratinocytes. At the same time, we also observed that DPP-4i promoted keratinocyte EMT indirectly through enhancement of SDF-1α expression in fibroblasts. Similar to our findings, DPP-4 has also been demonstrated to modulate SDF-1α in hematopoietic progenitor cell survival (42) and mobilization of progenitor cells (43). Moreover, SDF-1α promoted EMT and migration in breast cancer cells and hepatocellular carcinomas (35,36). Collectively, DPP-4i plays an important role in cooperation of skin cells during diabetic wound healing. Previous studies have revealed that the DPP-4 enzyme is critically involved in wound healing processes (22,23). Increased neovascularization and cell proliferation in the basal portion of the epidermis and connective tissue of corium, with enhanced IP-10, hypoxia inducible factor 1α (HIF-1α), and VEGF levels, as well as prompt macrophage recruitment were observed in DPP-$4^{-/-}$ mice (22). In addition, an important substrate of DPP-4, the chemotactic cytokine RANTES, was demonstrated to be highly induced in cutaneous wound margins,

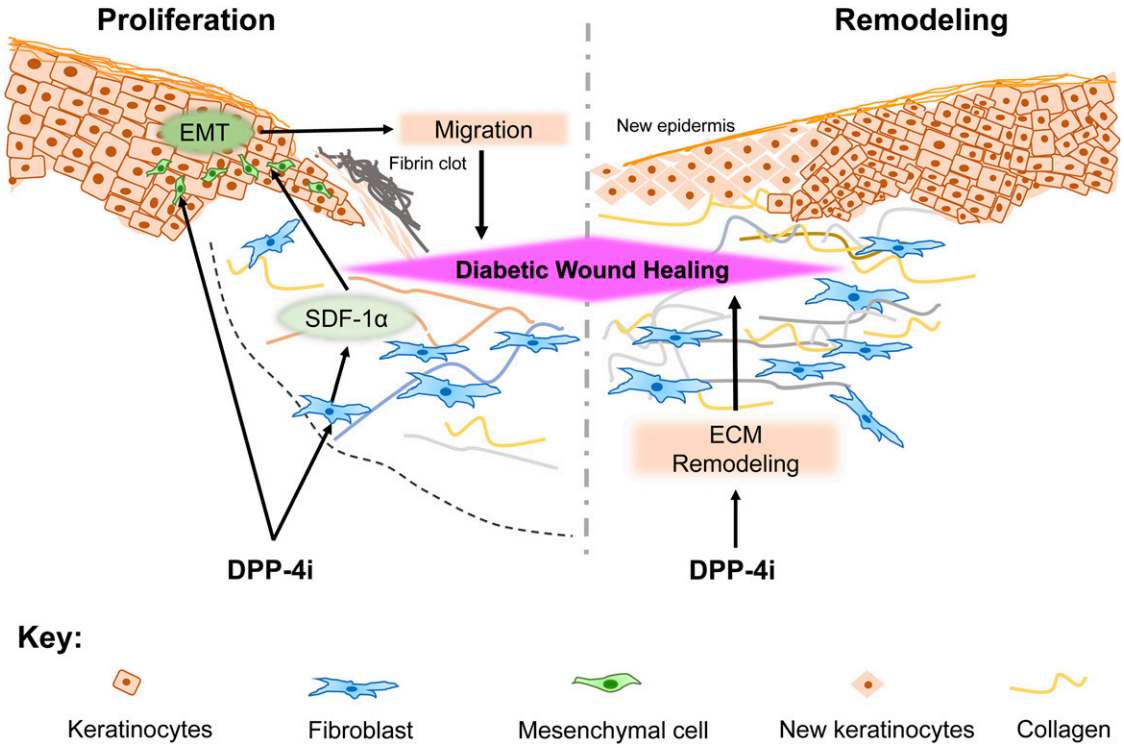

Figure 8—Scheme shows the working model. DPP-4i demonstrates a profound effect on keratinocytes and fibroblasts during proliferation and remodeling phases.

which resulted in monocytes infiltration and differentiation into activated macrophages (23). Therefore, future studies should elucidate potential mechanisms of DPP-4i in addition to EMT induction, such as potential substrates, the effect on the immune function and angiogenesis, even its off-target effects. Interestingly, our data showed the cells in the wound boundary appeared to be highly nonuniform, hinting at the possibility of leader cells (44,45), which are closely related with EMT occurrence and collective cell migration (46,47). Therefore, the effects of DPP-4i on the leader cells also need further investigation.

Recent studies have identified a role of DPP-4i in the activation of the NRF2 pathway (12,13). NRF2 has been shown to play an important protective role in various diabetic complications, including diabetic cardiomyopathy (48), diabetic nephropathy (49), and DUs, (16,17) by modulating antioxidant responses and attenuating oxidative stress (50). However, our results suggest that the promotive effect of DPP-4i treatment on diabetic wound repair was not primarily mediated through the NRF2 pathway. Moreover, the effect of DPP-4i was also independent of glycemic control, because 3 weeks of DPP-4i treatment did not reduce blood glucose levels in STZ-induced diabetic mice, which was consistent with the observations of Kanasaki et al. (10), Kim et al. (51), and Maida et al. (52). Taken together, these reports suggest very diverse functions and mechanisms of DPP-4i. Therefore, further studies should be recruited to explore additional potential functions and mechanisms of DPP-4i, such as modulation of oxidative stress.

Our findings also suggested that DPP-4i prevented excess accumulation of the ECM, which is related to scar formation in the remodeling phase. A recent study showed that the scar-forming fibroblasts selectively expressed DPP-4 and that inhibition of DPP-4 activity modulated ECM remodeling genes, such as COL1A1 and FN1, under physiological conditions (37,38). Combined with our observation in diabetes, DPP-4 might be a potential therapeutic target for abnormal scar formation.

Adult male mice were used in our study because they are used in most animal studies of diabetic wound healing (53–55). Male rodents are more susceptible to experimental hyperglycemia than females owing to the sex hormone profile (56,57), but whether sex influences the effect of DPP-4i still needs further investigation.

Overall, our study showed the pleiotropic effects of DPP-4i treatment on DUs and established the association of DPP-4is in coordinating cellular behaviors of skin cells to promote EMT and minimize scar formation. However, aside from the hypoglycemic function, few studies have reported the additional positive effect of other hypoglycemic drugs on DUs, suggesting the application of DPP-4is as a preferred option for treating DUs. Notably, some additional negative effects of DPP-4is have been reported, such as increased risks of tumor metastasis (12,13) and heart failure (4,5); therefore, DPP-4i administration in patients with diabetes with cancers or heart failure should be approached with caution. Furthermore, we suggest large-scale clinical trials of a series of clinically used DPP-4i medications to confirm

the value of its application in DUs, and we believe that such a trial will be helpful for developing clinical individualized treatment in the future.

Funding. This work was supported by the following grants: the National Natural Science Foundation of China (No. 81500647 to M.L., and No. 81471039 and No. 81270893 to H.Z.), the Natural Science Foundation Project of Chongqing (CSTC2016jcyjA0502 to M.L. and CSTC2014jcyjjq10006 and CSTC2012jjB10023 to H.Z.), the Third Military Medical University miaopu cultivation project, and Clinical Research Project of Xinqiao Hospital of Third Military Medical University (No. 2016YLC15 to M.L.).

Duality of Interest. No potential conflicts of interest relevant to this article were reported.

Author Contributions. M.L. contributed to study concept and design, analysis and interpretation of data, drafting of the manuscript, and study supervision and obtained study funding. L.C. contributed to acquisition of data, analysis and interpretation of data, statistical analysis, and drafting of the manuscript. W.L. and L.Z. contributed to acquisition of data and to analysis and interpretation of data. S.G. contributed to critical revision of the manuscript for important intellectual content. R.Z, Y.Z., X. Liu, M.W., X.Z., and X. Li contributed to acquisition of data. H.W. contributed to analysis and interpretation of data. L.L., Z.Z., and G.Y. contributed to study concept and design revision. M.L., L.C., W.L., L.Z., S.G., R.Z., Y.Z., X. Liu, M.W., X.Z., H.W., X. Li, L.L., Z.Z., G.Y., and H.Z. read and approved the manuscript for publication. H.Z. contributed to study concept and design revision, analysis and interpretation of data, and critical revision of the manuscript for important intellectual content; obtained study funding; and supervised the study. H.Z. is the guarantor of this work and, as such, had full access to all the data in the study and takes responsibility for the integrity of the data and the accuracy of the data analysis.

References

1. Marso SP, Daniels GH, Brown-Frandsen K, et al.; LEADER Steering Committee; LEADER Trial Investigators. Liraglutide and cardiovascular outcomes in type 2 diabetes. N Engl J Med 2016;375:311–322
2. Weber MA, Mansfield TA, Cain VA, Iqbal N, Parikh S, Ptaszynska A. Blood pressure and glycaemic effects of dapagliflozin versus placebo in patients with type 2 diabetes on combination antihypertensive therapy: a randomised, double-blind, placebo-controlled, phase 3 study. Lancet Diabetes Endocrinol 2016;4:211–220
3. Syngelaki A, Nicolaides KH, Balani J, et al. Metformin versus placebo in obese pregnant women without diabetes mellitus. N Engl J Med 2016;374:434–443
4. Scirica BM, Bhatt DL, Braunwald E, et al.; SAVOR-TIMI 53 Steering Committee and Investigators. Saxagliptin and cardiovascular outcomes in patients with type 2 diabetes mellitus. N Engl J Med 2013;369:1317–1326
5. Scirica BM, Braunwald E, Raz I, et al.; SAVOR-TIMI 53 Steering Committee and Investigators. Heart failure, saxagliptin, and diabetes mellitus: observations from the SAVOR-TIMI 53 randomized trial. Circulation 2014;130:1579–1588
6. Cefalu WT, Leiter LA, de Bruin TW, Gause-Nilsson I, Sugg J, Parikh SJ. Dapagliflozin's effects on glycemia and cardiovascular risk factors in high-risk patients with type 2 diabetes: a 24-week, multicenter, randomized, double-blind, placebo-controlled study with a 28-week extension. Diabetes Care 2015;38:1218–1227
7. Garber AJ, Abrahamson MJ, Barzilay JI, et al. American Association of Clinical Endocrinologists' comprehensive diabetes management algorithm 2013 consensus statement–executive summary. Endocr Pract 2013;19:536–557
8. Drucker DJ, Nauck MA. The incretin system: glucagon-like peptide-1 receptor agonists and dipeptidyl peptidase-4 inhibitors in type 2 diabetes. Lancet 2006;368:1696–1705
9. Tsuprykov O, Ando R, Reichetzeder C, et al. The dipeptidyl peptidase inhibitor linagliptin and the angiotensin II receptor blocker telmisartan show renal benefit by different pathways in rats with 5/6 nephrectomy. Kidney Int 2016;89:1049–1061
10. Kanasaki K, Shi S, Kanasaki M, et al. Linagliptin-mediated DPP-4 inhibition ameliorates kidney fibrosis in streptozotocin-induced diabetic mice by inhibiting endothelial-to-mesenchymal transition in a therapeutic regimen. Diabetes 2014;63:2120–2131
11. Shah Z, Kampfrath T, Deiuliis JA, et al. Long-term dipeptidyl-peptidase 4 inhibition reduces atherosclerosis and inflammation via effects on monocyte recruitment and chemotaxis. Circulation 2011;124:2338–2349
12. Wang H, Liu X, Long M, et al. NRF2 activation by antioxidant antidiabetic agents accelerates tumor metastasis. Sci Transl Med 2016;8:334ra351
13. Tschöp MH, Stumvoll M, Ristow M. Opposing effects of antidiabetic interventions on malignant growth and metastasis. Cell Metab 2016;23:959–960
14. Hur W, Gray NS. Small molecule modulators of antioxidant response pathway. Curr Opin Chem Biol 2011;15:162–173
15. Kumar H, Kim IS, More SV, Kim BW, Choi DK. Natural product-derived pharmacological modulators of Nrf2/ARE pathway for chronic diseases. Nat Prod Rep 2014;31:109–139
16. Long M, Rojo de la Vega M, Wen Q, et al. An essential role of NRF2 in diabetic wound healing. Diabetes 2016;65:780–793
17. Soares MA, Cohen OD, Low YC, et al. Restoration of Nrf2 signaling normalizes the regenerative niche. Diabetes 2016;65:633–646
18. Reinhold D, Vetter RW, Mnich K, et al. Dipeptidyl peptidase IV (DP IV, CD26) is involved in regulation of DNA synthesis in human keratinocytes. FEBS Lett 1998;428:100–104
19. Arwert EN, Mentink RA, Driskell RR, et al. Upregulation of CD26 expression in epithelial cells and stromal cells during wound-induced skin tumour formation. Oncogene 2012;31:992–1000
20. Barreira da Silva R, Laird ME, Yatim N, Fiette L, Ingersoll MA, Albert ML. Dipeptidylpeptidase 4 inhibition enhances lymphocyte trafficking, improving both naturally occurring tumor immunity and immunotherapy. Nat Immunol 2015;16:850–858
21. Van de Velde S, Hogan MF, Montminy M. mTOR links incretin signaling to HIF induction in pancreatic beta cells. Proc Natl Acad Sci U S A 2011;108:16876–16882
22. Baticic Pucar L, Pernjak Pugel E, Detel D, Varljen J. Involvement of DPP IV/CD26 in cutaneous wound healing process in mice. Wound Repair Regen 2017;25:25–40
23. Frank S, Kämpfer H, Wetzler C, Stallmeyer B, Pfeilschifter J. Large induction of the chemotactic cytokine RANTES during cutaneous wound repair: a regulatory role for nitric oxide in keratinocyte-derived RANTES expression. Biochem J 2000;347:265–273
24. Anon E, Serra-Picamal X, Hersen P, et al. Cell crawling mediates collective cell migration to close undamaged epithelial gaps. Proc Natl Acad Sci U S A 2012;109:10891–10896
25. Martin P. Wound healing–aiming for perfect skin regeneration. Science 1997;276:75–81
26. Falanga V. Wound healing and its impairment in the diabetic foot. Lancet 2005;366:1736–1743
27. Cheng F, Shen Y, Mohanasundaram P, et al. Vimentin coordinates fibroblast proliferation and keratinocyte differentiation in wound healing via TGF-β-Slug signaling. Proc Natl Acad Sci U S A 2016;113:E4320–E4327
28. Thielitz A, Vetter RW, Schultze B, et al. Inhibitors of dipeptidyl peptidase IV-like activity mediate antifibrotic effects in normal and keloid-derived skin fibroblasts. J Invest Dermatol 2008;128:855–866
29. Stoll SW, Rittié L, Johnson JL, Elder JT. Heparin-binding EGF-like growth factor promotes epithelial-mesenchymal transition in human keratinocytes. J Invest Dermatol 2012;132:2148–2157
30. Khamaisi M, Katagiri S, Keenan H, et al. PKCδ inhibition normalizes the wound-healing capacity of diabetic human fibroblasts. J Clin Invest 2016;126:837–853
31. Ashcroft GS, Dodsworth J, van Boxtel E, et al. Estrogen accelerates cutaneous wound healing associated with an increase in TGF-beta1 levels. Nat Med 1997;3:1209–1215
32. Bollag WB, Hill WD. CXCR4 in epidermal keratinocytes: crosstalk within the skin. J Invest Dermatol 2013;133:2505–2508

33. Li Y, Lei D, Swindell WR, et al. Age-associated increase in skin fibroblast-derived prostaglandin E2 contributes to reduced collagen levels in elderly human skin. J Invest Dermatol 2015;135:2181–2188
34. Ranzato E, Patrone M, Pedrazzi M, Burlando B. Hmgb1 promotes wound healing of 3T3 mouse fibroblasts via RAGE-dependent ERK1/2 activation. Cell Biochem Biophys 2010;57:9–17
35. Orimo A, Gupta PB, Sgroi DC, et al. Stromal fibroblasts present in invasive human breast carcinomas promote tumor growth and angiogenesis through elevated SDF-1/CXCL12 secretion. Cell 2005;121:335–348
36. Li X, Li P, Chang Y, et al. The SDF-1/CXCR4 axis induces epithelial–mesenchymal transition in hepatocellular carcinoma. Mol Cell Biochem 2014;392:77–84
37. Rinkevich Y, Walmsley GG, Hu MS, et al. Identification and isolation of a dermal lineage with intrinsic fibrogenic potential. Science 2015;348:aaa2151
38. Leavitt T, Hu MS, Marshall CD, Barnes LA, Lorenz HP, Longaker MT. Scarless wound healing: finding the right cells and signals. Cell Tissue Res 2016;365:483–493
39. Granstein RD, Flotte TJ, Amento EP. Interferons and collagen production. J Invest Dermatol 1990;95(Suppl.):75S–80S
40. Yamaguchi Y, Yoshikawa K. Cutaneous wound healing: an update. J Dermatol 2001;28:521–534
41. Leopold PL, Vincent J, Wang H. A comparison of epithelial-to-mesenchymal transition and re-epithelialization. Semin Cancer Biol 2012;22:471–483
42. Broxmeyer HE, Hoggatt J, O'Leary HA, et al. Dipeptidylpeptidase 4 negatively regulates colony-stimulating factor activity and stress hematopoiesis. Nat Med 2012;18:1786–1796
43. Di Marco GS, Reuter S, Kentrup D, et al. Cardioprotective effect of calcineurin inhibition in an animal model of renal disease. Eur Heart J 2011;32:1935–1945
44. Yang Y, Jamilpour N, Yao B, Dean ZS, Riahi R, Wong PK. Probing leader cells in endothelial collective migration by plasma lithography geometric confinement. Sci Rep 2016;6:22707
45. Omelchenko T, Vasiliev JM, Gelfand IM, Feder HH, Bonder EM. Rho-dependent formation of epithelial "leader" cells during wound healing. Proc Natl Acad Sci U S A 2003;100:10788–10793
46. Chapnick DA, Liu X. Leader cell positioning drives wound-directed collective migration in TGFβ-stimulated epithelial sheets. Mol Biol Cell 2014;25:1586–1593
47. Riahi R, Sun J, Wang S, Long M, Zhang DD, Wong PK. Notch1-Dll4 signalling and mechanical force regulate leader cell formation during collective cell migration. Nat Commun 2015;6:6556
48. Gu J, Cheng Y, Wu H, et al. Metallothionein is downstream of Nrf2 and partially mediates sulforaphane prevention of diabetic cardiomyopathy. Diabetes 2017;66:529–542
49. Zheng H, Whitman SA, Wu W, et al. Therapeutic potential of Nrf2 activators in streptozotocin-induced diabetic nephropathy. Diabetes 2011;60:3055–3066
50. Jaramillo MC, Zhang DD. The emerging role of the Nrf2-Keap1 signaling pathway in cancer. Genes Dev 2013;27:2179–2191
51. Kim SJ, Nian C, Doudet DJ, McIntosh CH. Dipeptidyl peptidase IV inhibition with MK0431 improves islet graft survival in diabetic NOD mice partially via T-cell modulation. Diabetes 2009;58:641–651
52. Maida A, Hansotia T, Longuet C, Seino Y, Drucker DJ. Differential importance of glucose-dependent insulinotropic polypeptide vs glucagon-like peptide 1 receptor signaling for beta cell survival in mice. Gastroenterology 2009;137:2146–2157
53. Lucas T, Schäfer F, Müller P, Eming SA, Heckel A, Dimmeler S. Light-inducible antimiR-92a as a therapeutic strategy to promote skin repair in healing-impaired diabetic mice. Nat Commun 2017;8:15162
54. Randeria PS, Seeger MA, Wang XQ, et al. siRNA-based spherical nucleic acids reverse impaired wound healing in diabetic mice by ganglioside GM3 synthase knockdown. Proc Natl Acad Sci U S A 2015;112:5573–5578
55. Marrotte EJ, Chen DD, Hakim JS, Chen AF. Manganese superoxide dismutase expression in endothelial progenitor cells accelerates wound healing in diabetic mice. J Clin Invest 2010;120:4207–4219
56. Ostenson CG, Grill V, Roos M. Studies on sex dependency of B-cell susceptibility to streptozotocin in a rat model of type II diabetes mellitus. Exp Clin Endocrinol 1989;93:241–247
57. Oliveira RB, Maschio DA, Carvalho CP, Collares-Buzato CB. Influence of gender and time diet exposure on endocrine pancreas remodeling in response to high fat diet-induced metabolic disturbances in mice. Ann Anat 2015;200:88–97